Advanced Powder Technology 31 (2020) 4470–4481

Contents lists available at ScienceDirect

Advanced Powder Technology

journal homepage: www.elsevier.com/locate/apt

Original Research Paper

Free convective melting-solidification heat transfer of nano-encapsulated phase change particles suspensions inside a coaxial pipe

Mohammad Ghalambaz [a,b], S.A.M Mehryan [c], Nemat Mashoofi [d], Ahmad Hajjar [e], Ali J. Chamkha [f,g,*], Mikhail Sheremet [h], Obai Younis [i,j]

[a] Metamaterials for Mechanical, Biomechanical and Multiphysical Applications Research Group, Ton Duc Thang University, Ho Chi Minh City, Vietnam
[b] Faculty of Applied Sciences, Ton Duc Thang University, Ho Chi Minh City, Vietnam
[c] Young Researchers and Elite Club, Yasooj Branch, Islamic Azad University, Yasooj, Iran
[d] Faculty of Mechanical and Energy Engineering, Shahid Beheshti University, Tehran, Iran
[e] ECAM Lyon, LabECAM, Université de Lyon, Lyon, France
[f] Institute of Research and Development, Duy Tan University, Da Nang 550000, Vietnam
[g] Institute of Theoretical and Applied Research (ITAR), Duy Tan University, Hanoi 100000, Vietnam
[h] Laboratory on Convective Heat and Mass Transfer, Tomsk State University, Tomsk, Russia
[i] Department of Mechanical Engineering, College of Engineering at Wadi Addwaser, Prince Sattam Bin Abdulaziz University, Saudi Arabia
[j] Department of Mechanical Engineering, Faculty of Engineering, University of Khartoum, Sudan

ARTICLE INFO

Article history:
Received 21 May 2020
Received in revised form 26 August 2020
Accepted 24 September 2020
Available online 17 October 2020

Keywords:
Nano-Encapsulated Phase Change Material (NEPCM)
Melting
Solidification
Natural convection

ABSTRACT

The nano encapsulated phase change materials are of the great energy storage potential in various engineering applications. Since they are new nanomaterials, new models for understanding their thermal behavior and capability are essential. This work aims to investigate the unsteady thermal behavior of Nano-Encapsulated Phase Change Material (NEPCM) suspensions in a cylindrical cavity. The particles contain a Phase Change Material (PCM) core, which can absorb/release a substantial amount of thermal energy upon phase change. The phase change particles are well dispersed in a liquid fluid and freely move along with the fluid. The flow, heat transfer, and the particle phase change were modeled using partial differential equations. A non-dimensional approach was employed to generalize the study. The unsteady charging and discharging behavior of the NEPCM suspension are investigated for the volume fraction of the NEPCM particles, fusion temperature of nanoparticles, Stefan number, and the Rayleigh number. Numerical results show that an increment in the Stefan number, i.e., *Ste*, can significantly reduce the Nusselt number, i.e., Nu_a, at the charging mode of the system. However, the dependency of the Nu_a at the discharging mode on the *Ste* is negligible. Also, it was found that the effect of the fusion temperature of the particle's core (θ_f) on heat transfer depends on the working mode of the system. In the charging mode, using a higher value of θ_f decreases the heat transfer rate. Reversibly, a higher value of θ_f inhibits the Nu_a during discharging state. Furthermore, the results show that for $Ra = 10^6$, $Ste = 0.2$, and $\theta_f = 0.1$, a rise of ϕ from 0 to 0.05 leads in about 1.73 and 1.55 times of improvement in the value of Nu_a for the cases of the melting and solidification of the core of NEPCM particles.

1. Introduction

The Nano-Encapsulated Phase Change Material (NEPCM) suspensions represent an advanced type of nanofluids, in which the nanoparticle's core can undergo a phase change and absorb/release a significant amount of latent heat as a constant fusion temperature. The high surface area of tiny nanoparticles improves the heat transfer between the base fluid and the phase change material (PCM) inside the nanoparticles. The liquid containing NEPCM particles flows in a system, and releases/absorbs heat in the form of latent heat upon phase change. Hence, a suspension of NEPCM particles has a promising practical interest in many heat transfer and thermal energy storage systems.

The synthesis of NEPCM particles and suspensions has been the subject of some recent researches. Sari et al. [1] produced nano-encapsulated phase change particles made of

* Corresponding author.
E-mail addresses: mohammad.ghalambaz@tdtu.edu.vn (M. Ghalambaz), ahmad.hajjar@ecam.fr (A. Hajjar), alichamkha@duytan.edu.vn (A.J. Chamkha), sheremet@math.tsu.ru (M. Sheremet).

https://doi.org/10.1016/j.apt.2020.09.022
0921-8831/

Nomenclature

Latin letters

C_p	specific heat in constant pressure (J/kg K)
Cr	ratio of total heat capacity of the suspension to the base fluid
f	normalized fusion function
g	gravitational acceleration (m s^{-2})
H	height of the enclosure
h_{sf}	latent heat of the core of NEPCM particles
k	thermal conductivity (W m^{-1} K^{-1})
Nc	conductivity number
Nu	Nusselt number
Nv	viscosity number
P	pressure (Pa)
P	normalized pressure
Pr	Prandtl number
r	horizontal Cartesian coordinate (m)
R	normalized horizontal Cartesian coordinate
Ra	Rayleigh number
Ste	Stefan number
t	dimensional time (s)
T	temperature (°C)
T_{Mr}	melting temperature window
u_r	r-velocity component (m s^{-1})
U_R	R-normalized velocity component
u_z	z-velocity component (m s^{-1})
U_Z	Z-normalized velocity component
z	vertical Cartesian coordinate (m)
Z	normalized vertical Cartesian coordinate

Greek symbols

μ	fluid viscosity (kg s m^{-1})
α	thermal diffusivity (m^{-2} s)
β	coefficient of thermal expansion (K^{-1})
δ	normalized fusion range
θ	scaled temperature
ι	weight ratio of core to shell
λ	ratio of the heat capacity of the NEPCM particles to the host fluid
ρ	density (kg/m^3)
τ	non-dimensional time
ϕ	volume concentration of particles
Ψ	stream function

Subscript

b	suspension
c	cold wall
co	particle's core
f	host fluid
fu	fusion
h	hot wall
p	NEPCM nanoparticles
sh	particle's shell

polymethylmethacrylate (PMMA) shells. The core of nanoparticles was a mixture of octacosane (C28)–heptadecane (C17), and the nanoparticle's shell/core mass ratio was 1:2. The fusion temperature of NEPCM particles was about 21 °C, with a latent heat of 98000 J/kg. Wu et al. [2] successfully synthesized NEPCMS using lauric acid and carbon nanotubes, while Shi et al. [3] proposed a novel one-step method for the preparation of NEPCM particles in the range of 200–400 nm. The nanoparticles were made of paraffin and PMMA as the phase change core and the shell, respectively. About 53% weight of the nanoparticles was a phase change core with a latent melting heat of 64.93 J/g.

Some of the potential applications of NEPCMs have been explored in recent researches. For instance, Heydarian et al. [4] examined the thermal performance of using a suspension of NEPCM-water in a heat pipe. It was found that using the NEPCM suspension enhances the heat transfer and reduces the thermal resistance of a pulsating heat pipe. Li et al. [5] utilized a slurry of NEPCMs-water in a metal foam for passive thermal management applications and found 38% heat transfer improvement. Alehosseini and Jafari [6] reviewed the application of NEPCM particles in the food industry and reported that the encapsulation of phase change material prevents leakage of phase change material during processing or packaging.

The passive heat transfer and energy storage of NEPCM suspensions usually occur in enclosures. Thus, the phase change heat transfer of phase change materials (PCMs) without encapsulation has been the subject of various recent investigations. Mehryan et al. [7] studied the melting phase change behavior of nano-enhanced phase change materials in a cavity. The PCM was made of n-octadecane-mesoporous silica (MPSiO2). The presence of these particles induces non-Newtonian behavior in molten PMC, and it was found that using mesoporous silica could not improve the melting heat transfer in the cavity. The effect of the magnetic field [8,9], metal foam [10], and non-Newtonian phase change [11] have also been investigated. Moreover, neglecting the phase change effects, many aspects of heat transfer in enclosures such as entropy generation [12], conjugate heat transfer [13,14], double-diffusive mixed convection [15,16], porous media [17], magnetohydrodynamic effects [18,19], and nanofluids [20,21], have been addressed in recent studies.

The presence of NEPCMs particles influences the thermophysical properties and thermal behavior of the suspensions. Thus, developing new theoretical models for understanding natural convection heat transfer of NEPCM suspensions is highly demanded. Such models could provide a basic understanding and design tool for promoting the applications of these novel materials.

At present, the natural convection heat transfer of NEPCMs suspensions has been investigated in very few studies. Ghalambaz et al. [22,23] modeled the steady-state free convection heat transfer of NEPCMs suspensions in a regular [22] and tilted cavity [23]. The top and bottom cavity were insulated, but the side walls were isothermal with different temperatures. The influences of the fusion temperature of nanoparticles, latent heat capacity, and volume fraction of nanoparticles were investigated on the enhancement of heat transfer. The results show that using NEPCMs particles could enhance the heat transfer, and there was an optimum fusion temperature for maximum heat transfer enhancement. Moreover, in the case of a tilted cavity [23], the dimensionless phase change temperature of 0.5 and the tilted angle of 42° could lead to maximum heat transfer rate.

Following Ghalambaz et al. [22], Hajjar et al. [24] investigated the transient heat transfer of NEPCMs in a cavity in the same geometrical configuration. The results indicated that the fusion temperature of NEPCMs is a crucial factor, which could notably influence the heat transfer rate. Moreover, the volume fraction of NEPCMs is another important factor. For instance, a 2.5% rise in the volume fraction of NEPCMs enhanced the heat transfer by 21%. Mehryan et al. [25] explored the effect of using NEPCMs in an eccentric annulus cavity. It was found that the fusion

temperature equal to the mean temperature of the hot and cold surfaces could lead to a maximum heat transfer rate.

The transient natural convection of NEPCMs suspensions embedded in a glass-ball porous medium was explored by Ghalambaz et al. [26] in a square cavity. The results demonstrated that there is an optimum range of fusion temperatures for maximum enhancement of heat transfer. The raise of NEPCM particles enhances the heat transfer rate. Moreover, the relation between the porosity and volume fraction of nanoparticles was not monotonic, and there is an optimal concentration for a specific porosity. The steady-state mixed convection heat transfer of NEPCMs was also investigated in the boundary layer flow over a flat plate embedded in a porous medium [27]. It was found that the presence of phase change particles would enhance the heat transfer, and the presence of an optimum fusion temperature was also confirmed in mixed convection boundary layer flows.

The literature review shows that the natural convection heat transfer of NEPCM suspensions has been investigated in previous studies, either under steady-state [22,23,27] or unsteady state [24–26] conditions. The steady-state investigation of NEPCMs is only capable of analyzing the thermal behavior of NEPCMs. However, the energy storage of NEPCMs occurs during a time interval and requires an unsteady approach. In [22–27], there was a temperature difference across the enclosure or free stream, and hence, the heat transfer was a combination of a charging and a discharging process along with heat transfer enhancement. Thus, the energy storage and energy discharge process of NEPCMs suspension were not clear. This research aims to address the charging and discharging process of NEPCMs in an enclosure for the first time.

2. Material and methods

A coaxial pipe occupied with a Newtonian suspension is studied as the problem physics. The host fluid of the suspension is water, and the NEPCM particles are the dispersed nanoparticles. As indicated in Fig. 1 (a) and (b), the inner pipe having the height of H and the radius of r_o is heated or cooled at the temperature of T_h or T_c, respectively. However, the outer pipe is well insulated. Depending on the temperature of the inner surface, the initial temperature of the suspension can be T_h or T_c. T_{fu}, the melting point temperature of the core of the NEPCM particles, is between the higher and lower temperatures. Hence, it is obvious that the core of the NEPCMs particles undergoes the melting or solidification process. The ratio of the outer radius to the inner one is R_r. The thermophysical properties of the making materials of the NEPCM particles are tabulated in Table 1.

2.1. The formulation

The mass conservation of the incompressible fluid inside the coaxial pipe is governed by the following equation:

$$\frac{1}{r}\frac{\partial(ru_r)}{\partial r}+\frac{\partial u_z}{\partial z}=0 \tag{1}$$

Also, the momentum conservation of the Newtonian and laminar flow is governed by the following equations:

$$\rho_b\left(\frac{\partial u_r}{\partial t}+u_r\frac{\partial u_r}{\partial r}+u_z\frac{\partial u_r}{\partial z}\right)=-\frac{\partial p}{\partial r}+\frac{\mu_b}{r}\frac{\partial}{\partial r}\left(r\frac{\partial u_r}{\partial r}\right)-\frac{\mu_b u_r}{r^2}+\mu_b\frac{\partial^2 u_r}{\partial z^2} \tag{2-a}$$

$$\rho_b\left(\frac{\partial u_z}{\partial t}+u_r\frac{\partial u_z}{\partial r}+u_z\frac{\partial u_z}{\partial z}\right)=-\frac{\partial p}{\partial z}+\frac{\mu_b}{r}\frac{\partial}{\partial r}\left(r\frac{\partial u_z}{\partial r}\right)+\mu_b\frac{\partial^2 u_z}{\partial z^2}+g\rho_b\beta_b(T-T_c) \tag{2-b}$$

Finally, the heat transfer inside the NEPCM suspension is governed by the following equation:

$$(\rho C_p)_b\left(\frac{\partial T}{\partial t}+u_r\frac{\partial T}{\partial r}+u_z\frac{\partial T}{\partial z}\right)=\frac{k_b}{r}\frac{\partial}{\partial r}\left(r\frac{\partial T}{\partial r}\right)+k_b\frac{\partial^2 T}{\partial z^2} \tag{3}$$

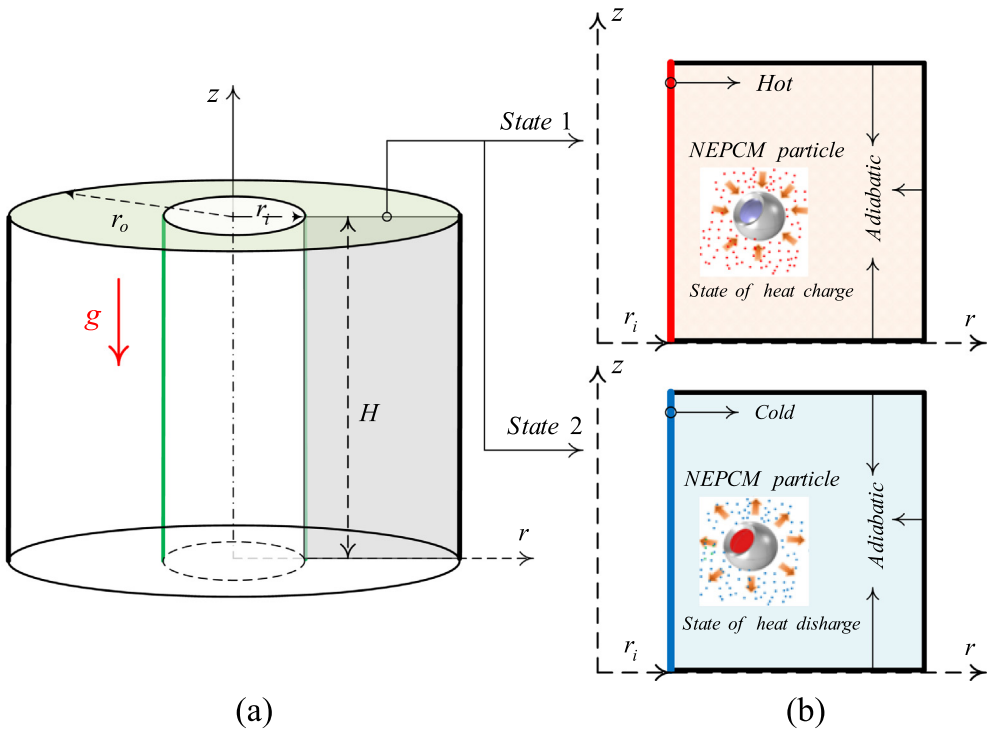

Fig. 1. (a): schematic configuration of the problem physics, and (b): heat charge and discharge states of NEPCM particles.

Table 1
Thermophysical properties of the base fluid and NEPCM particles [29].

Properties	Water (base fluid)	Polyurethane (shell)	Nonadecane (core)
C_p (KJ/Kg K)	4179	1317.7	2037
ρ (Kg/m^3)	997.1	786	721
k (W/m K)	0.613	–	–
β (K^{-1})	21×10^{-5}	17.28×10^{-5}	–
μ (kg/m s)	8.9×10^{-4}	–	–
h_{sf} (kJ/kg)	–	–	211
T_{fu} (°C)	–	–	32

The boundary conditions imposed are formulated as follows:

$$\forall\ r,\ z,\ t\ |r = r_i,\ 0 \leqslant z \leqslant H\ \&\ t \geqslant 0\ \ \Rightarrow u_r = u_z = 0,\ T = T_w$$
$$T_w = \begin{cases} T_h\ Charging\ mode \\ T_c\ Disharging\ mode \end{cases} \tag{4-a}$$

$$\forall\ r,\ z,\ t\ \left|\begin{array}{l} z = 0,\ r_i \leqslant r \leqslant r_o\ \&\ t \geqslant 0 \\ z = H,\ r_i \leqslant r \leqslant r_o\ \&\ t \geqslant 0 \end{array}\right\} \Rightarrow u_r = u_z = 0,\ \frac{\partial T}{\partial z} = 0 \tag{4-b}$$

$$\forall\ r,\ z,\ t\ |r = r_o,\ 0 \leqslant z \leqslant H\ \&\ t \geqslant 0 \Rightarrow u_r = u_z = 0,\ \frac{\partial T}{\partial r} = 0 \tag{4-c}$$

Also, the initial condition is as follows:

$$\forall\ r,\ z,\ t\ |\ r_i < r < r_o,\ 0 < z < H\ \&\ t = 0\ \ \Rightarrow u_r = u_z = 0,\ T = T_i$$
$$T_i = \begin{cases} T_c\ Charging\ mode \\ T_h\ Disharging\ mode \end{cases} \tag{4-d}$$

2.2. Thermophysical properties of the suspension

It is evident that the thermophysical properties of the suspension are functions of its making components. The density of the suspension is [28]:

$$\rho_b = (1-\phi)\rho_f + \phi\rho_p \tag{5}$$

p and f of the above relation belong to the particles and the host liquid. The density of NEPCM particles is [22]:

$$\rho_p = (1+\imath)(\rho_{sh} + \imath\rho_{co})^{-1}\rho_{co}\rho_{sh},\ \imath = \rho_{sh}^{-1}\rho_{co} \tag{6}$$

in which $\imath \sim 0.447$ [29]. The specific heat capacity of the suspension is [30,31]:

$$C_{p,b} = \phi\rho_p\rho_b^{-1}C_{p,eff,p} + (1-\phi)\rho_f C_{p,f}\rho_b^{-1} \tag{7}$$

For the NEPCM particles with no the phase change process, $C_{p,eff,p}$ is equal to the sensible heat, i.e. $C_{p,p}$. In contrary, the latent heat of the core plays an important role in determining the specific heat capacity of the NEPCM particles during phase change [28,32]:

$$C_{p,eff,p} = C_{p,p} + \left\{\frac{\pi}{2}\cdot\left(\frac{h_{sf}}{T_{Mr}} - C_{p,p}\right)\cdot\sin\left(\pi\frac{T - T_{fu} + T_{Mr}/2}{T_{Mr}}\right)\right\}\gamma$$
$$\gamma = \begin{cases} 0 & T < T_{fu} - T_{Mr}/2 \\ 1 & T_{fu} - T_{Mr}/2 < T < T_{fu} + T_{Mr}/2 \\ 0 & T > T_{fu} + T_{Mr}/2 \end{cases} \tag{8}$$

in which, $T_{Mr} = T_1 - T_0$ is the melting temperature window of the core of the NEPCM particles. T_0 and T_1 are respectively the solidus and liquidus temperatures of the NEPCM core. The coefficient of volumetric thermal expansion of the suspension is [31]:

$$\beta_b = (1-\phi)\beta_f + \phi\beta_p \tag{9}$$

The thermal conductivity of the suspension can be achieved as [33,34]:

$$k_b = k_f + k_f Nc\phi \tag{10-a}$$

in which, Nc is the thermal conductivity number. Also, the dynamic viscosity of the suspension are calculated as follows [33,34]

$$\mu_b = \mu_f + \mu_f Nv\phi \tag{10-b}$$

Nv of the above relation is the dynamic viscosity number.

2.3. Normalized form of the equations and boundary conditions

To normalize the equations which describe the natural convection flow, the variables presented below are applied:

$$R = \frac{r}{H},\ Z = \frac{z}{H},\ R_i = \frac{r_i}{H},\ R_o = \frac{r_o}{H},\ U_R = \frac{u_r H}{\alpha_f}$$
$$U_Z = \frac{u_z H}{\alpha_f},\ P = \frac{pH^2}{\rho_f\alpha_f^2},\ \theta = \frac{T - T_c}{\Delta T},\ \tau = \frac{t\alpha_f}{H^2} \tag{11}$$

in which, $\Delta T = T_h - T_c$. Hence, we then have:

$$\frac{1}{R}\frac{\partial(RU_R)}{\partial R} + \frac{\partial U_Z}{\partial Z} = 0 \tag{12}$$

$$\left(\frac{\rho_b}{\rho_f}\right)\left(\frac{\partial U_R}{\partial\tau} + U_R\frac{\partial U_R}{\partial R} + U_Z\frac{\partial U_R}{\partial Z}\right) = -\frac{\partial P}{\partial R} + \frac{Pr}{R}\left(\frac{\mu_b}{\mu_f}\right)\frac{\partial}{\partial R}\left(R\frac{\partial U_R}{\partial R}\right)$$
$$-Pr\left(\frac{\mu_b}{\mu_f}\right)\frac{U_R}{R^2} + Pr\left(\frac{\mu_b}{\mu_f}\right)\frac{\partial^2 U_R}{\partial Z^2} \tag{13}$$

$$\left(\frac{\rho_b}{\rho_f}\right)\left(\frac{\partial U_Z}{\partial\tau} + U_R\frac{\partial U_Z}{\partial R} + U_Z\frac{\partial U_Z}{\partial Z}\right) = -\frac{\partial P}{\partial Z} + Pr\left(\frac{\mu_b}{\mu_f}\right)\frac{1}{R}\frac{\partial}{\partial R}\left(R\frac{\partial U_Z}{\partial R}\right)$$
$$+Pr\left(\frac{\mu_b}{\mu_f}\right)\frac{\partial^2 U_Z}{\partial Z^2} + PrRa\left(\frac{\beta_b}{\beta_f}\right)\theta \tag{14}$$

in which, Rayleigh number (Ra) and Prandtl number (Pr) are:

$$Ra = \frac{g\rho_f\beta_f\Delta TH^3}{\alpha_f\mu_f},\ Pr = \frac{\mu_f}{\rho_f\alpha_f} \tag{15}$$

Ra indicates the relative significance of the buoyancy forces with respect to the viscous forces, and Pr is the ratio of the momentum diffusivity to the thermal diffusivity.

Also,

$$\left(\frac{\beta_b}{\beta_f}\right) = (1-\phi) + \phi\left(\frac{\beta_p}{\beta_f}\right),\quad \left(\frac{\rho_b}{\rho_f}\right) = (1-\phi) + \phi\left(\frac{\rho_p}{\rho_f}\right) \tag{16}$$

In this work, the thermal expansion of the particles and water are presumed to be the same, therefore, $\beta_b/\beta_f = 1$.

$$Cr\left(\frac{\partial\theta}{\partial\tau} + U_R\frac{\partial\theta}{\partial R} + U_Z\frac{\partial\theta}{\partial Z}\right) = \left(\frac{k_b}{k_f}\right)\frac{1}{R}\frac{\partial\theta}{\partial R} + \left(\frac{k_b}{k_f}\right)\frac{\partial^2\theta}{\partial R^2} + \left(\frac{k_b}{k_f}\right)\frac{\partial^2\theta}{\partial Z^2} \tag{17}$$

where

$$Cr = \frac{(\rho C_p)_b}{(\rho C_p)_f} = (1-\phi) + \phi\lambda + \frac{\phi}{\delta\,Ste}f \tag{18}$$

Here, Cr depicts the ratio of the sum of the sensible and latent heats of the nanoliquid to that of the pure fluid. In fact, as previously mentioned, the core of the NEPCM particles dispersed inside the base fluid can undergo the phase change process; hence, the latent

heat of the NEPCM particles is involved in the stored energy in the mixture. The normalized parameters in *Cr* are:

$$Ste=\frac{(\rho C_p)_f(\rho_{sh}+\imath\rho_{co})\Delta T}{\alpha_f(h_{sf}\rho_{co}\rho_{sh})},\ \delta=\frac{T_{Mr}}{\Delta T},\ \lambda=\frac{(C_{p,co}+\imath C_{p,sh})\rho_{co}\rho_{sh}}{(\rho C_p)_f(\rho_{sh}+\imath\rho_{co})} \tag{19}$$

are, respectively, Stefan number (*Ste*), which is the ratio of the sensible heat to the latent heat, the normalized melting temperature window δ, and the sensible heat capacity ratio of the NEPCM particle to the host fluid λ. f, the normalized fusion function, is:

$$f=\tfrac{\pi}{2}\sin\left(\tfrac{\pi}{\delta}(\theta-\theta_{fu}+\delta/2)\right)\sigma$$
$$\sigma=\begin{cases}0 & \theta<\theta_{fu}-\delta/2\\ 1 & \theta_{fu}-\frac{\delta}{2}<\theta<\theta_{fu}+\delta/2\\ 0 & \theta>\theta_{fu}+\delta/2\end{cases} \tag{20}$$

θ_{fu} of the above relation is the fusion temperature:

$$\theta_{fu}=\frac{T_{fu}-T_c}{\Delta T} \tag{21}$$

The normalized form of the imposed initial and boundary conditions are:

$$\forall\ R,\ Z,\ \tau\mid R=R_i,\ 0\leqslant Z\leqslant 1\ \&\ \tau\geqslant 0\ \Rightarrow U_R=U_Z=0,\ \theta=\theta_w$$
$$\theta_w=\begin{cases}1\ \textit{Charging mode}\\ 0\ \textit{Disharging mode}\end{cases} \tag{22-a}$$

$$\forall\ R,\ Z,\ \tau\ \left|\begin{array}{l}Z=0,\ R_i\leqslant R\leqslant R_o\ \&\ \tau\geqslant 0\\ Z=1,\ R_i\leqslant R\leqslant R_o\ \&\ \tau\geqslant 0\end{array}\right\}\Rightarrow\ U_R=U_Z=0,\ \frac{\partial\theta}{\partial Z}=0 \tag{22-b}$$

$$\forall\ R,\ Z,\ \tau\ \left|R=R_o,\ 0\leqslant Z\leqslant 1\ \&\ \tau\geqslant 0\Rightarrow\ U_R=U_Z=0,\ \frac{\partial\theta}{\partial R}=0\right. \tag{22-c}$$

$$\forall\ R,\ Z,\ \tau\mid R_i<\ R\ <R_o,\ 0<\ Z\ <1\ \&\ \tau=0\ \Rightarrow U_R=U_Z=0,\ \theta=\theta_i$$
$$\theta_i=\begin{cases}0\ \textit{Charging mode}\\ 1\ \textit{Disharging mode}\end{cases} \tag{4-d}$$

The average Nusselt number, Nu_a, is used to evaluate the heat transferred through the inner wall:

$$Nu_a=(1+Nc\phi)\int_0^{\tau}\int_0^{1}\left|\left(\frac{\partial\theta}{\partial R}\right)_{R=R_i}\right|dZ\,d\tau \tag{23}$$

It is worth noting that the temperature gradient on the inner wall is positive and negative for the heating and cooling processes, respectively. However, for the sake of graphical illustrations, the heat transfer rate through the inner wall, the absolute value is used. To better visualize the suspension flow inside the coaxial pipe, the streamlines are presented:

$$\frac{1}{R}\frac{\partial^2\Psi}{\partial R^2}-\frac{1}{R^2}\frac{\partial\Psi}{\partial R}+\frac{1}{R}\frac{\partial^2\Psi}{\partial Z^2}=-\left(\frac{\partial U_R}{\partial Z}-\frac{\partial U_Z}{\partial R}\right) \tag{24}$$

The boundary condition for the streamlines is the Dirichlet boundary condition with zero value at the walls.

3. Numerical approach and grid test

Due to the nonlinear nature of the coupled equations described in the previous section, the use of a powerful numerical approach to obtain the results is inevitable. Hence, a finite element code was developed for numerical simulations. The developed code details in [35]. A structured mesh was used to describe the domain of the solution. The mesh is dense near the walls to better capture gradients near the wall. Prior to extracting the numerical results, a grid independence test was conducted to ensure the numerical precision. Fig. 2 display an example of a coarse structured mesh for demonstration purpose. The utilized mesh for the computations is much finer. As depicted in Fig. 3, the average Nusselt number studied in several meshes with various sizes to obtain the optimum mesh size when *Ste* = 0.2, *Ra* = 10^7, θ_f = 0.1, *Pr* = 6.2, and ϕ = 0.05. Some fluctuations of Nusselt number can be seen in the case of a coarse grid of 50 × 50. Indeed, this coarse grid size cannot adequately capture the phase change area and leads to high computational error. The use of a grid of 150 × 150 ensures that the numerical experiments are almost independent of the mesh size with a reasonable computational cost. Hence, the grid size of 150 × 150 was selected for computations.

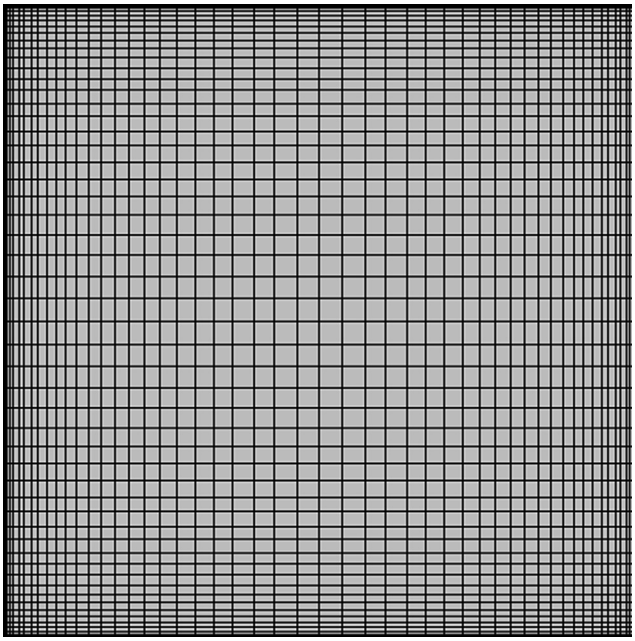

Fig. 2. An example of a coarse structured mesh.

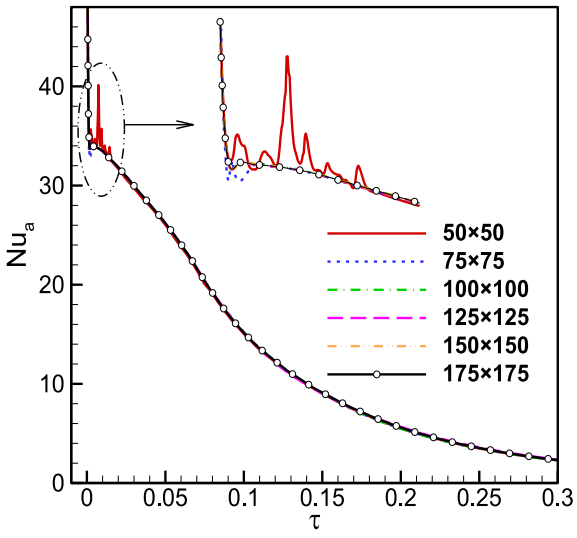

Fig. 3. Grid independence for Nusselt Number versus time.

Two previous published investigations were utilized to verify the numerical technique employed in the current work. The geometrical conditions, along with the non-dimensional parameters applied in the verification study, were similar to those in the references [36,37]. In the first verification, the outcomes presented by Kahveci [36] on the natural convection of a suspension of the water and TiO_2 particles flowing in a square enclosure were utilized in the verification investigation. The predicted average Nusselt number for the current work at different values of nanoparticles volume fraction was evaluated with the results from Kahveci [36]. The excellent precision obtained, as illustrated by Fig. 4 depicts a reliable verification of the model developed in the current work for simulating the natural convection of a suspension. In the second verification, the numerical measurements by Xu et al. [37] on the transient non-dimensional temperature of a pure fluid flowing within an enclosure partitioned by a thin vertical wall at a certain point are also employed to verify this study. The left and right sidewalls are kept at low and high temperatures of T_c and T_h. At $t = 0$, the initial temperatures of the fluid on the left and right sides of the partition is T_c and T_h. The numerical data by Xu et al. [37], which presented for the transient variations of temperature at the specified point of (−0.025, 0.375) are compared with our results. As depicted in Fig. 5, the discrepancy between the results of the two studies is very slight. In this verification, Pr = 6.63, and $Ra = 9.2 \times 10^8$.

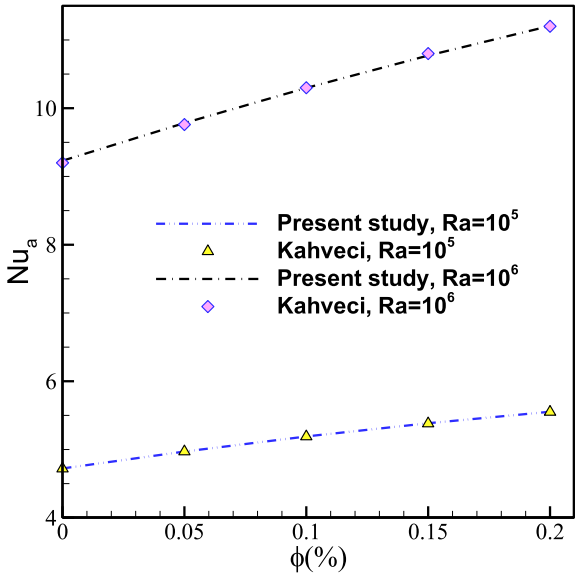

Fig. 4. The average Nusselt (Nu_a) as a function of the volume fraction of NEPCM particles at two different Ra numbers [36].

4. Results and discussion

This research investigates the free convection behavior of a NEPCM suspension in annuli of the eccentric horizontal cylinders. Hee, the dynamic viscosity and thermal conductivity numbers are adopted as Nv = 12.5 and Nc = 23.8. The sensible heat capacity ratio λ is 0.32 [29]. The numerical analysis is conducted for the alterable parameters, including the Stefan number $0.2 \le Ste \le 0.8$, Rayleigh number $10^4 \le Ra \le 10^6$, normalized fusion temperature $0.05 \le \theta_f \le 1$, and the NEPCM volume fraction $0.0 \le \phi \le 5\%$. Here, the total time of fully charge/discharge, i.e., τ_f, is considered as a scale for reporting the outcomes. The subscripts of s and m indicate the total discharging time (solidification) and total charging time (melting), respectively.

Fig. 6 depicts the streamlines, the isotherms, and the maps of the heat capacity ratio, i.e., Cr, in the cavity in the charging mode. The particle's core is initially in the solid phase with a uniformly cold temperature. During the charging process, the hot wall maintains hot, and the NEPCM suspension commences to absorb the heat in the form of sensible and latent heat. Here, τ_f = 0.4530 denotes the total time of the charging process, in which all of the nanoparticles reach the liquid state.

Fig. 6(a) exhibits the field contours after 10% τ_f. As seen, due to the heat of the inner hot tube, the temperature distribution advances toward the top and right section of the cavity, but still, most regions of the right and bottom part of the cavity are at initial cold temperature. The streamlines depict the formation of a weak natural convection flow. The red area in Cr contour indicates the particle's phase transitions. Hence, the red area can be considered as the phase change area. Here, 0.97 inside Cr contours depicts the ratio of the total heat capacity of the nanoliquid to that of the pure fluid when the nanoparticles do not experience the phase change process. In the ribbon zone, the nano-encapsulated phase change

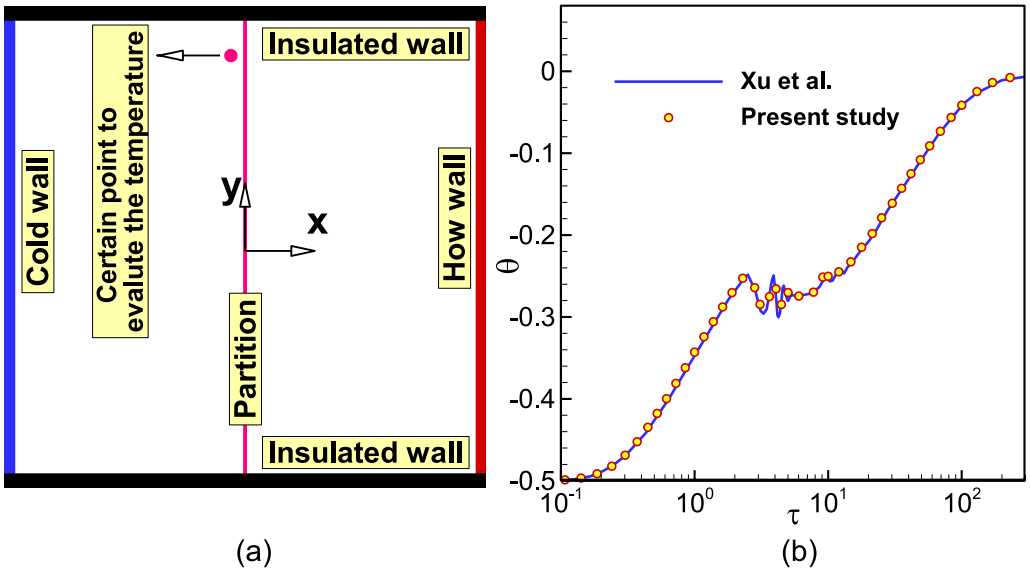

Fig. 5. (a): schematic view of the used geometry for verification, and (b): dimensionless temperature against time at specified point [37] for Pr = 6.63, and $Ra = 9.2 \times 10^8$.

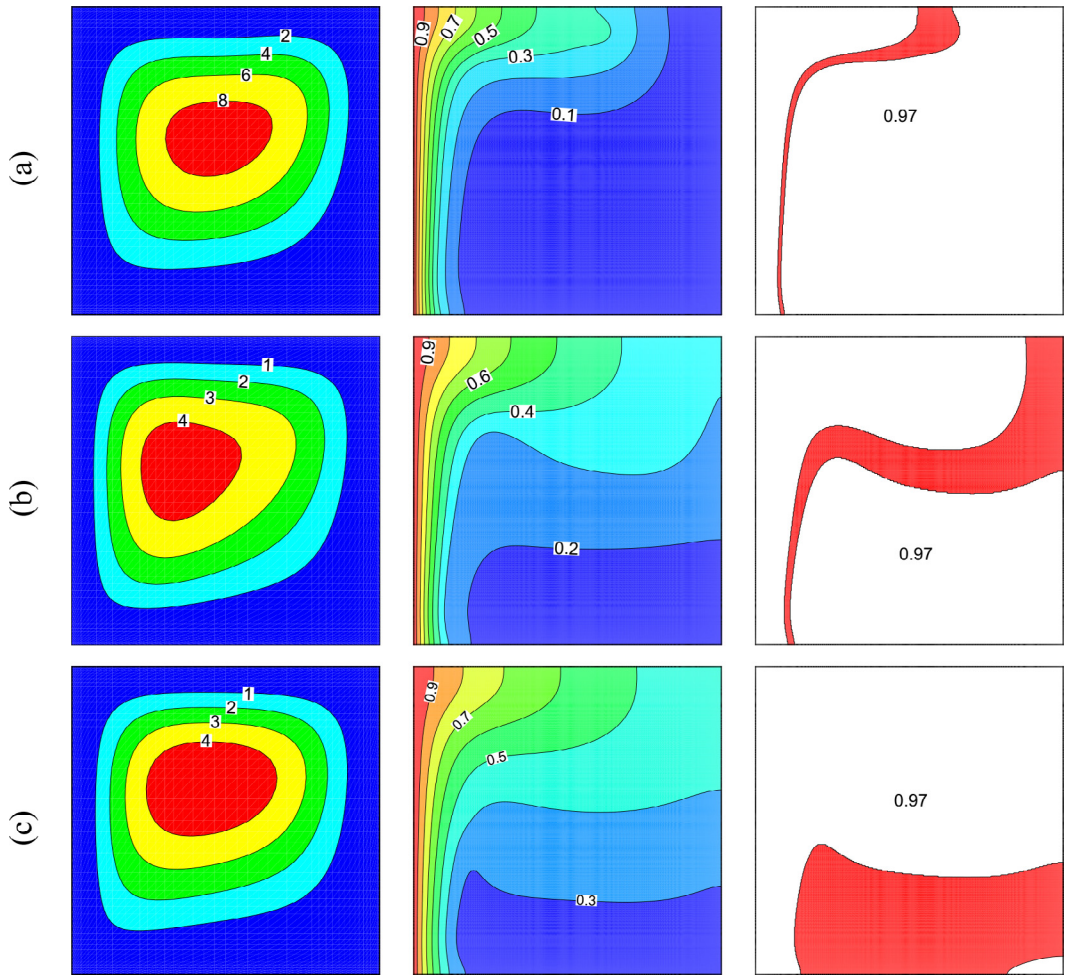

Fig. 6. Streamlines and contours of temperature and capacity ratio (Cr) for (a): τ = 10% τ_f, (b): τ = 40% τ_f, and (c): τ = 70% τ_f where total melting time (τ_f) is 0.1822 when Ste = 0.2, Ra = 10^5, θ_f = 0.3, and ϕ = 0.05.

particles undergo the melting/solidification process and the $Cr \neq 0.97$.

Attention to the temperature contour shows that the phase change area laid around the temperature level of θ = 0.3, which is equal to the fusion temperature of NEPCM particles. The NEPCM particles above the Cr area (red area) are in fully charged in a liquid state, and the NEPCM particles below this area are untouched and in a fully solid-state yet.

Fig. 6(b) shows that the temperature gradient more advances toward the right and develops toward the bottom areas of the cavity as time elapses. There is a larger area above the phase change area, which depicts that a larger amount of NEPCM particles are fully charged. The convection strength is weakening as the distance between streamlines is increased. This is because there is no cold wall in the cavity, and the increase of the overall temperature of the suspension reduces the temperature differences and, consequently, the buoyancy forces and natural convection. Fig. 6(c) shows the advancement of heat transfer in the cavity when the charging time reaches 70% of the total charging time. The average temperature in the cavity is increased at every point. The temperature distribution affects the region of the cavity at which phase change occurs. The right down part of the cavity is in the solid-state while the other part has already melted. In this case, most of the particles are in a fully liquid state, and most of the remaining particles are in the red area and under phase change.

Fig. 7 shows the same results as Fig. 6 but for the case of discharging. In this case, the NEPCM particles are initially at a hot temperature, and the cold wall is maintained at a cold temperature. During the discharging process, the buoyancy-driven flow occurs in the cavity initially due to the temperature difference between the cold inner tube and the hot suspension surrounding it. As the temperature of the suspension rises, the temperature difference between the cold wall and the suspension decreases, reducing, thus, the intensity of the convective flow.

The cold isotherms are initially concentrated near the inner tube, and, as time goes on, the overall temperature of the suspension decreases. The concentration of the isotherms is reduced, and isothermal contours corresponding to cold temperatures cover the cavity. The Cr contours follow the variation of the temperature distribution in the cavity. PCM melting occurs near the isotherm corresponding to θ_f, and consequently, its location moves toward the right as time goes on. When 70% of the total melting time, the portion of the suspension containing the liquid NEPCM is focused in the upper right part of the cavity, while the solid-NEPCM particles cover the other parts.

Fig. 8 shows the variation of the average Nusselt number Nu_a as a function of time during charging and discharging modes for various volume fraction of the NEPCM particles ϕ. The same variation of Nu_a is observed in the charging and discharging modes. In both cases, Nu_a elevates with the growth of ϕ and is maximum for ϕ

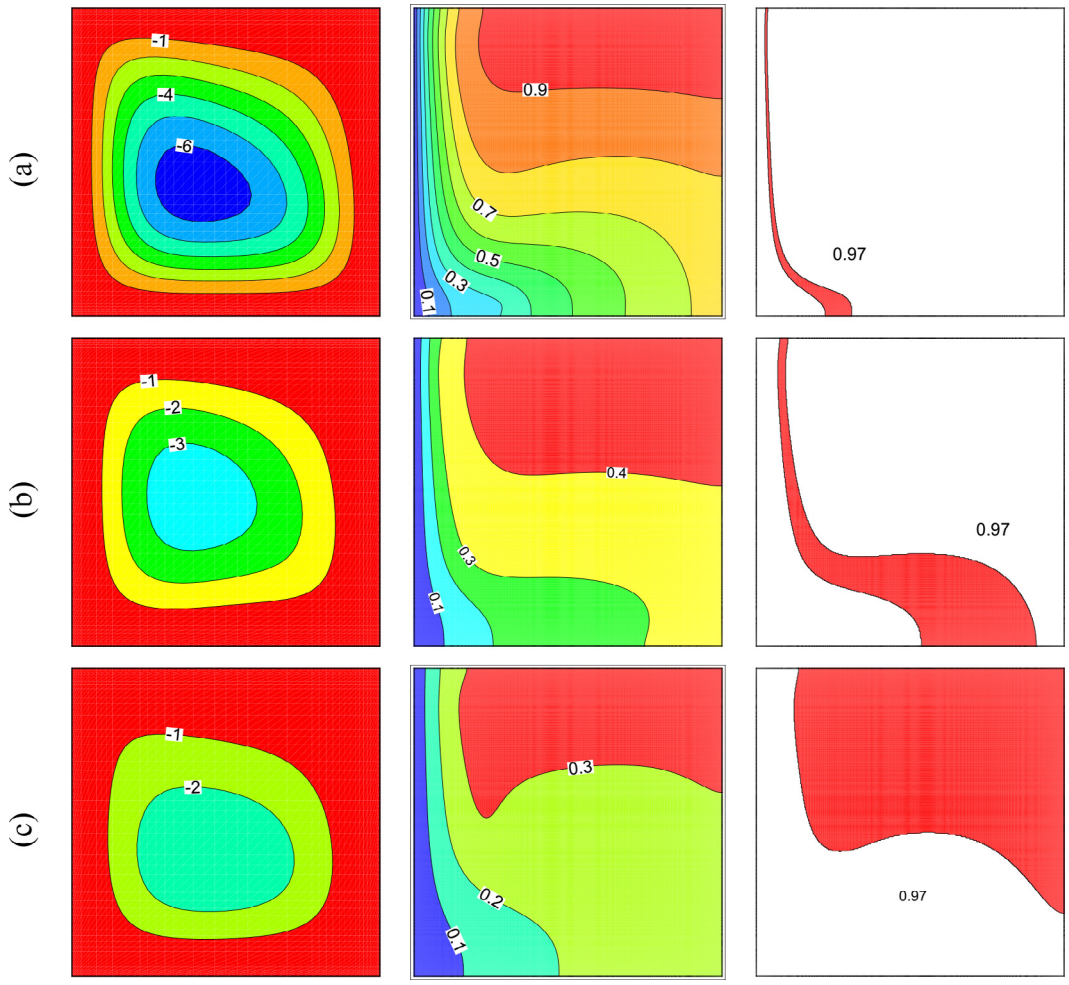

Fig. 7. Streamlines and Contours of temperature and capacity ratio (*Cr*) for (a): τ = 10% τ_f, (b): τ = 40% τ_f, and (c): τ = 70% τ_f where total solidification time (τ_f) is 0.4530 when *Ste* = 0.2, *Ra* = 10^5, θ_f = 0.3, and ϕ = 0.05.

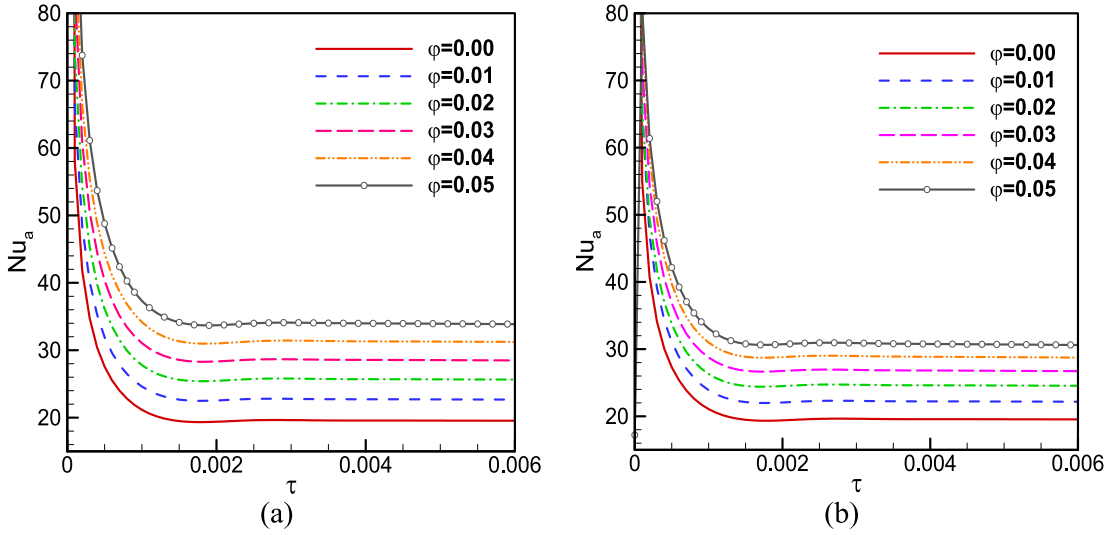

Fig. 8. The variations of average Nusselt number versus the time for different values of volume fraction of NEPCM particles in the case of *Ra* = 10^6, *Ste* = 0.2, and θ_f = 0.1 for (a): charging process and (b): discharging process.

= 5%. A rise of ϕ from 0 to 0.05 leads in about 1.73 and 1.55 times of improvement in the value of Nu_a for gthe cases of the melting and solidification of the core of NEPCM particles. Indeed, the involvement of the particles to the heat transfer grows when their volume fraction is increased, as more particles are undergoing a phase change, and more latent heat is participating in the overall heat

Table 2
The effects of volume fraction on the total time of melting and solidification when Ste = 0.2, Ra = 10^6, and θ_f = 0.1.

$\tau_{f,\,m}$	$\tau_{f,\,s}$	ϕ
0.0000	0.0000	0.00
0.0805	0.6466	0.01
0.0808	0.6573	0.02
0.0816	0.6641	0.03
0.0821	0.6728	0.04
0.0823	0.6802	0.05

Table 3
The effects of Rayleigh number on the total time of melting and solidification when Ste = 0.2, θ_f = 0.1, and ϕ = 0.05.

$\tau_{f,\,m}$	$\tau_{f,\,s}$	Ra
0.2035	1.7883	10^4
0.1271	1.1475	10^5
0.0823	0.6802	10^6

transfer occurring in the cavity. As a result, the more NEPCM particles, the more enhancement of the heat transfer rate and a higher value of Nu_a.

Table 2 presents the total time of phase change of the NEPCM core during melting ($\tau_{f,\,m}$) and solidification ($\tau_{f,\,s}$) for different values of ϕ. It is shown that the total time of melting is greater in the case of solidification. This is due to the selected value of θ_f during the calculations. The second observation is that the total melting and solidification times increase when a higher value of ϕ is used. In fact, the total phase change time depends directly on the volume fraction of the NEPCM particles. When more NEPCM particles are added to the suspension, the time required for the total phase change of all these particles increases as more particles are required to undergo a phase change. In conclusion, raising ϕ rises the heat transfer in the cavity and increases the total time of melting or solidification.

The effect of Rayleigh number Ra on the variation of Nu_a as a function of time during charging and discharging is illustrated in Fig. 9. Using a higher value of Ra increases the value of Nu_a during charging and discharging modes. In both modes, the maximum heat transfer is achieved for Ra = 10^6. A slightly higher value is obtained in the charging mode. Raising Ra from 10^4 to 10^6 increases by up to 3 times the value of Nu_a. This is since Ra is an indicator of the relative importance of the flow buoyancy forces. As Ra is increased, the intensity of the buoyancy forces grows, and the heat transfer by convection is enhanced. Consequently, a higher value of Nu_a is obtained.

The effect of Ra on the total time of melting during charging and solidification during discharging is shown in Table 3. Increasing Ra reduces the total melting time in charging mode and the total solidification time in discharging mode substantially. As early mentioned, the increased intensity of the buoyancy forces leads to an enhancement of the convective heat transfer and, thus, a stronger flow circulation, and eventually, an extensive phase change occurs in the NEPCM suspension. Therefore, the total melting or solidification time decreases for a higher value of Ra.

Fig. 10 illustrates the variation of Nu_a as a function of non-dimensional time for various values of the NEPCM fusion temperature (θ_f) during charging and discharging processes. It can be seen that while in charging mode, a higher value of Nu_a is obtained when θ_f is reduced, the opposite occurs in discharging mode where reducing θ_f tends to decrease Nu_a. In fact, when θ_f is increased, the temperature difference between the hot inner cylinder and θ_f during charging decreases, and the zone of the cavity where the initial temperature is higher than θ_f is reduced. As the melting of the NEPCM core takes place in that zone of the cavity, less NEPCM particles would undergo a phase change, and their contribution to the overall heat transfer is diminished.

Conversely, in the discharging mode, increasing θ_f raises the difference between the temperature of the cold inner cylinder and θ_f and enlarges the zone of the cavity where the NEPCM particles would initially undergo solidification. In that case, the heat transfer is enhanced. None-the-less, in both modes, Fig. 10 shows that the effect of θ_f on the value of Nu_a remains relatively limited, as only a 10% difference is observed between the maximum and minimum values of Nu_a when θ_f is varied in both modes. It should be noted that the Nusselt profiles are reported at initial times, and a much longer time is required for fully charged or discharged cases of the enclosure.

The total time of melting and solidification during charging and discharging for different values of θ_f is presented in Table 4. It is shown that increasing θ_f reduces the total solidification time

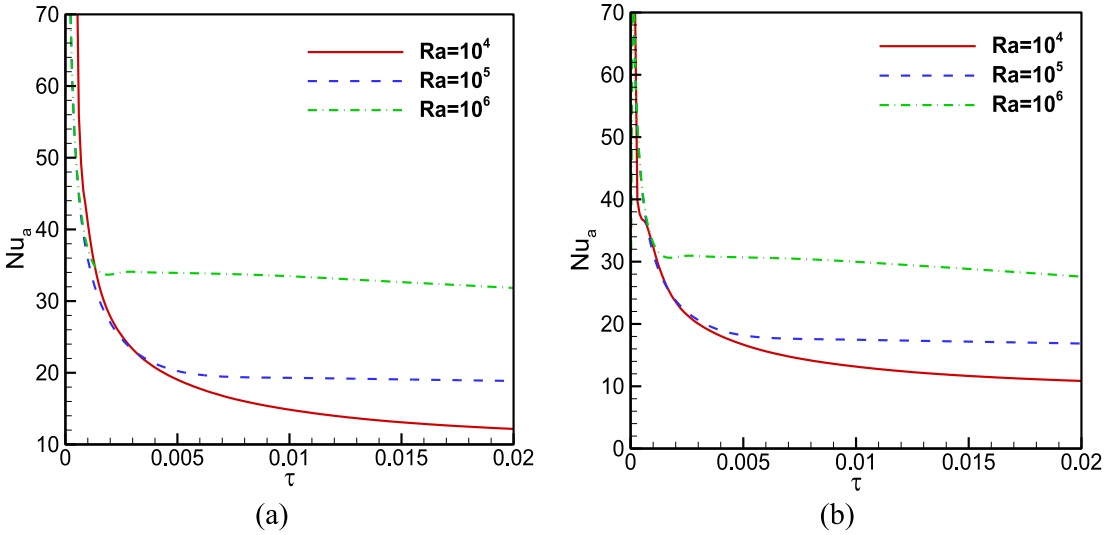

Fig. 9. The variations of average Nusselt number versus the time for different values of Rayleigh Number when Ste = 0.2, θ_f = 0.1, and ϕ = 0.05 for (a): charging and (b) discharging states.

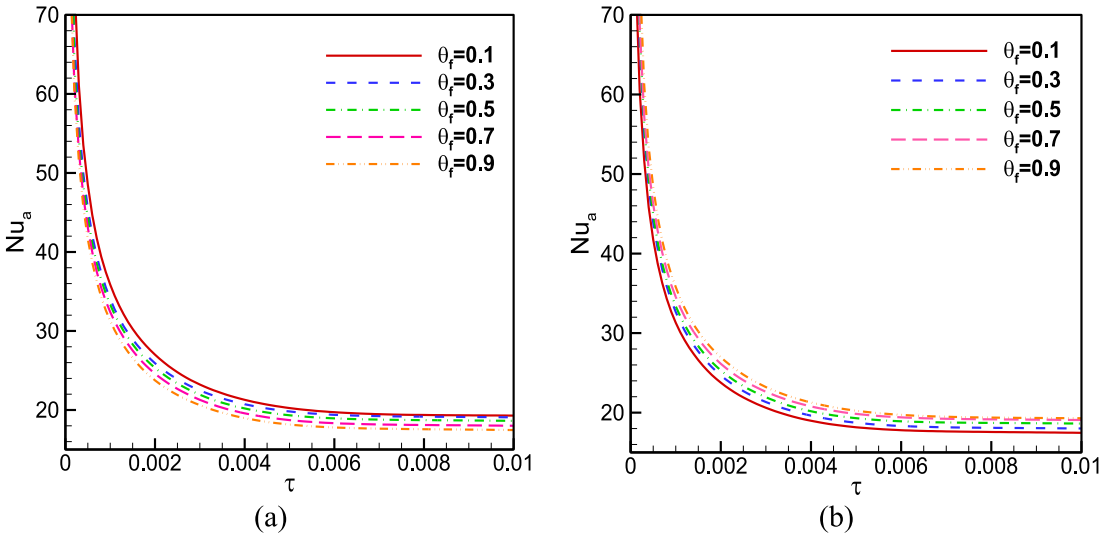

Fig. 10. The variations of average Nusselt number versus the time for different values of fusion/solidification temperature of NEPCM particles when $Ra = 10^6$, $St = 0.2$, $\phi = 0.05$ for (a): charging and (b) discharging states.

Table 4
The effects fusion/solidification temperature on the total time of melting and solidification when $Ste = 0.2$, $Ra = 10^6$, and $\phi = 0.05$.

$\tau_{f,\,m}$	$\tau_{f,\,s}$	θ_f
0.1271	1.1475	0.1
0.1822	0.4530	0.3
0.2781	0.2743	0.5
0.4612	0.1866	0.7
1.1326	0.1243	0.9

during discharging. Inversely, the total melting time is reduced during charging when the value of θ_f is decreased. This is also related to the temperature difference between the inner cylinder and θ_f. In charging mode, when θ_f is increased, the initial zone that would undergo melting is smaller. More time is then needed for all the NEPCM particles to undergo melting and, as a result, the total melting time increases. On the other hand, during discharging, the opposite occurs, and the total solidification time is reduced when θ_f is increased.

The time history of the Nusselt number for different values of Stefan number during charging and discharging is illustrated in Fig. 11. It can be seen that the value of Nu_a increases when the value of *Ste* is reduced. Indeed, *Ste* describes the ratio of sensible heat to latent heat during phase change. A higher value of *Ste* indicates a decrease in the relative importance of latent heat and the contribution of the phase change of the particle's cores to the overall heat transfer in the cavity. A lower value of Nu_a is therefore obtained in that case. It should be noted that this effect is less apparent in the discharging mode, where varying the value of *Ste* seems to have minimal impact on Nu_a. This is due to the value used for the fusion temperature ($\theta_f = 0.1$), which is very close to the temperature of the cold wall and already limiting the influence of the particles to the heat transfer.

Table 5 presents the total time of phase change in charging and discharging modes for various values of *Ste*. It is found that increas-

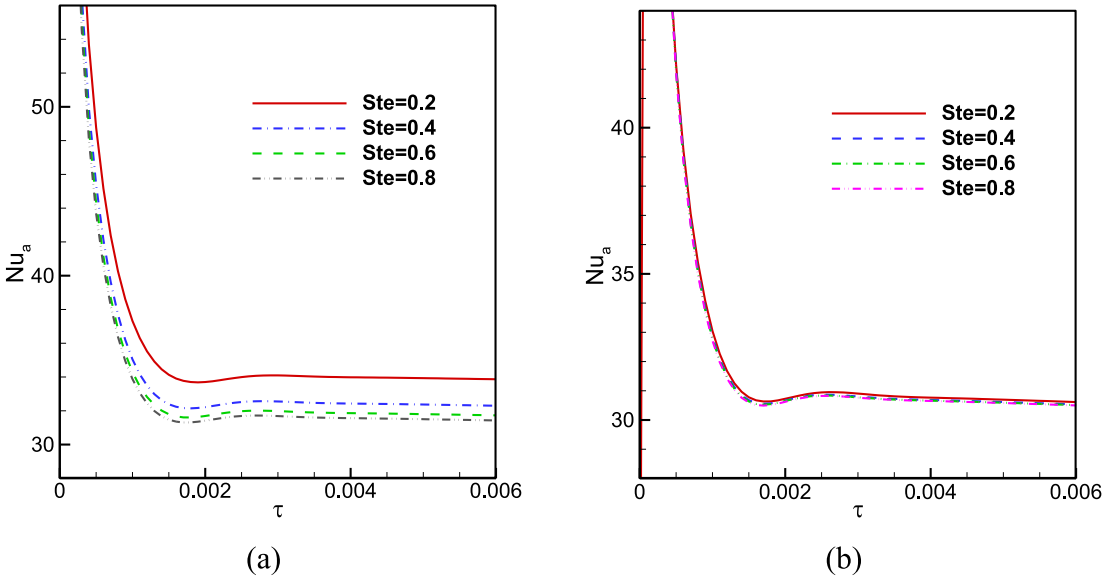

Fig. 11. The time history of the average Nusselt number for various values of *Ste* when $Ra = 10^6$, $\theta_f = 0.1$, $\phi = 0.05$ for (a): charging and (b) discharging states.

Table 5
The effects Stephan Number on the total time of melting and solidification when $Ra = 10^6$, $\theta_f = 0.1$, and $\phi = 0.05$.

Ste	$\tau_{f,\,s}$	$\tau_{f,\,m}$
0.2	0.6801	0.0823
0.4	0.5402	0.0654
0.6	0.4900	0.0580
0.8	0.4615	0.0558

ing *Ste* reduces the total melting time during charging and the total solidification time in the discharging mode. Certainly, when *Ste* increases, the latent heat of the NEPCM core is decreased, and less heat is required for the core to undergo a phase change, and, consequently, the total phase change time is reduced.

5. Conclusion

The charging and discharging behavior of a cylindrical enclosure filled with a suspension of NEPCMs were addressed theoretically. The phase change particles participate in heat transfer and absorb/store a significant amount of thermal energy on phase change. The effects of essential parameters of the NEPCM suspension, such as the non-dimensional fusion temperature, volume fraction of nanoparticles, and the Stefan number on the flow and heat transfer, were investigated. The main results of the present numerical study could be summarized as follows:

- Using a higher value of the nanoparticle's volume fraction enhances heat transfer. Using a 5% volume fraction enhances by up to 1.73 and 1.55 times the heat transfer inside the cavity compared to the case of a pure fluid for the cases of the melting and solidification of the core of NEPCM particles, due to the increased contribution of the particles to the total heat transfer. As the number of the NEPCM particles increases, the total melting or solidification time increases as more particles should undergo a phase change.
- The effect of the fusion temperature θ_f of the particle's core on heat transfer depends on the temperature of the inner cylinder. In the charging mode, when the inner cylinder is hot, using a higher value of θ_f reduces the difference between it and the temperature of the cylinder and, consequently, decreases the initial melting zone in the cavity. Heat transfer is inhibited in that case. A similar behavior but in the opposite direction occurs during discharging. In the latter case, heat transfer is improved when θ_f is increased. In addition, raising θ_f increases the total melting time during charging and reduces the total solidification time during discharging.
- Raising the value of the Stefan number *Ste* reduces the relative importance of the latent heat of the NEPCM and decreases their participation in the overall heat transfer in the cavity. Consequently, the heat transfer is inhibited when a higher value of *Ste* is used. Due to the decrease of the latent heat for a higher *Ste*, the total charging/discharging time in the two modes is decreased.

Declaration of Competing Interest

The authors declare that they have no known competing financial interests or personal relationships that could have appeared to influence the work reported in this paper.

References

[1] A. Sarı, C. Alkan, C. Bilgin, A. Bicer, Preparation, characterization and thermal energy storage properties of micro/nano encapsulated phase change material with acrylic-based polymer, Polym. Sci. B 60 (2018) 58–68.
[2] S. Wu, X. Ma, D. Peng, Y. Bi, The phase change property of lauric acid confined in carbon nanotubes as nano-encapsulated phase change materials, J. Therm. Anal. Calorim. 136 (2019) 2353–2361.
[3] J. Shi, X. Wu, R. Sun, B. Ban, J. Li, J. Chen, Nano-encapsulated phase change materials prepared by one-step interfacial polymerization for thermal energy storage, Mater. Chem. Phys. 231 (2019) 244–251.
[4] R. Heydarian, M.B. Shafii, A.R. Shirin-Abadi, R. Ghasempour, M.A. Nazari, Experimental investigation of paraffin nano-encapsulated phase change material on heat transfer enhancement of pulsating heat pipe, J. Therm. Anal. Calorim. 137 (2019) 1603–1613.
[5] W. Li, D. Zhang, T. Jing, M. Gao, P. Liu, G. He, F. Qin, Nano-encapsulated phase change material slurry (Nano-PCMS) saturated in metal foam: a new stable and efficient strategy for passive thermal management, Energy 165 (2018) 743–751.
[6] E. Alehosseini, S.M. Jafari, Micro/nano-encapsulated phase change materials (PCMs) as emerging materials for the food industry, Trends Food Sci. Technol. (2019).
[7] S. Mehryan, M. Vaezi, M. Sheremet, M. Ghalambaz, Melting heat transfer of power-law non-Newtonian phase change nano-enhanced n-octadecane-mesoporous silica (MPSiO2), Int. J. Heat Mass Transf. 151 (2020) 119385.
[8] S. Mehryan, A. Tahmasebi, M. Izadi, M. Ghalambaz, Melting behavior of phase change materials in the presence of a non-uniform magnetic-field due to two variable magnetic sources, Int. J. Heat Mass Transf. 149 (2020) 119184.
[9] M. Ghalambaz, S.M.H. Zadeh, S. Mehryan, K.A. Ayoubloo, N. Sedaghatizadeh, Non-Newtonian behavior of an electrical and magnetizable phase change material in a filled enclosure in the presence of a non-uniform magnetic field, Int. Commun. Heat Mass Transfer 110 (2020) 104437.
[10] M. Ghalambaz, J. Zhang, Conjugate solid-liquid phase change heat transfer in heatsink filled with phase change material-metal foam, Int. J. Heat Mass Transf. 146 (2020) 118832.
[11] M. Ghalambaz, K.A. Ayoubloo, A. Hajjar, Melting heat transfer of a non-Newtonian phase change material in a cylindrical vertical-cavity partially filled porous media, Int. J. Numer. Meth. Heat Fluid Flow (2019).
[12] M.H.S. Alnajem, A.I. Alsabery, I. Hashim, Entropy generation and natural convection in a wavy-wall cavity filled with a nanofluid and containing an inner solid cylinder, IOP Conference Series: Materials Science and Engineering, IOP Publishing (2019) 032044.
[13] A. Alsabery, M. Yazdi, A. Altawallbeh, I. Hashim, Effects of nonhomogeneous nanofluid model on convective heat transfer in partially heated square cavity with conducting solid block, J. Therm. Anal. Calorim. 136 (2019) 1489–1514.
[14] F.M. Azizul, A.I. Alsabery, I. Hashim, Heatlines visualisation of mixed convection flow in a wavy heated cavity filled with nanofluids and having an inner solid block, Int. J. Mech. Sci. 175 (2020) 105529.
[15] A.Q.A. Al-Hassan, M.A. Ismael, Numerical study of double diffusive mixed convection in horizontal channel with composite open porous cavity, Special Top. Rev. Porous Media: Int. J. 10 (2019).
[16] M.A. Ismael, Double-diffusive mixed convection in a composite porous enclosure with arc-shaped moving wall: tortuosity effect, J. Porous Media 21 (2018).
[17] A.I. Alsabery, R. Roslan, J. Al-Smail, I. Hashim, Effects of internal heat generation and partial heating on transient natural convection in an inclined porous cavity using LTNE model, J. Porous Media 23 (2020).
[18] H.K. Hamzah, F.H. Ali, M. Hatami, D. Jing, Effect of two baffles on MHD natural convection in U-shape superposed by solid nanoparticle having different shapes, J. Appl. Computat. Mech. (2020).
[19] K. Periyadurai, M. Selvan, D.-H. Doh, Impact of magnetic field on convective flow of a micropolar fluid with two parallel heat source, J. Appl. Computat. Mech. 5 (2019) 652–666.
[20] M.A. Sadiq, A.I. Alsabery, I. Hashim, MHD mixed convection in a lid-driven cavity with a bottom trapezoidal body: two-phase nanofluid model, Energies 11 (2018) 2943.
[21] S. Mehryan, E. Izadpanahi, M. Ghalambaz, A. Chamkha, Mixed convection flow caused by an oscillating cylinder in a square cavity filled with Cu–Al 2 O 3/water hybrid nanofluid, J. Therm. Anal. Calorim. 137 (2019) 965–982.
[22] M. Ghalambaz, A.J. Chamkha, D. Wen, Natural convective flow and heat transfer of nano-encapsulated phase change materials (NEPCMs) in a cavity, Int. J. Heat Mass Transf. 138 (2019) 738–749.
[23] M. Ghalambaz, S. Mehryan, I. Zahmatkesh, A. Chamkha, Free convection heat transfer analysis of a suspension of nano–encapsulated phase change materials (NEPCMs) in an inclined porous cavity, Int. J. Therm. Sci. 157 (2020) 106503.
[24] A. Hajjar, S. Mehryan, M. Ghalambaz, Time periodic natural convection heat transfer in a nano-encapsulated phase-change suspension, Int. J. Mech. Sci. 166 (2020) 105243.
[25] S. Mehryan, M. Ghalambaz, L.S. Gargari, A. Hajjar, M. Sheremet, Natural convection flow of a suspension containing nano-encapsulated phase change particles in an eccentric annulus, J. Storage Mater. 28 (2020) 101236.
[26] M. Ghalambaz, S. Mehryan, A. Hajjar, A. Veisimoradi, Unsteady natural convection flow of a suspension comprising Nano-Encapsulated Phase

Change Materials (NEPCMs) in a porous medium, Adv. Powder Technol. 31 (2020) 954–966.
[27] M. Ghalambaz, T. Groşan, I. Pop, Mixed convection boundary layer flow and heat transfer over a vertical plate embedded in a porous medium filled with a suspension of nano-encapsulated phase change materials, J. Mol. Liq. 293 (2019) 111432.
[28] L. Chai, R. Shaukat, L. Wang, H.S. Wang, A review on heat transfer and hydrodynamic characteristics of nano/microencapsulated phase change slurry (N/MPCS) in mini/microchannel heat sinks, Appl. Therm. Eng. 135 (2018) 334–349.
[29] S. Barlak, O.N. Sara, A. Karaipekli, S. Yapıcı, Thermal conductivity and viscosity of nanofluids having nanoencapsulated phase change material, Nanoscale Microscale Thermophys. Eng. 20 (2016) 85–96.
[30] B. Chen, X. Wang, R. Zeng, Y. Zhang, X. Wang, J. Niu, Y. Li, H. Di, An experimental study of convective heat transfer with microencapsulated phase change material suspension: laminar flow in a circular tube under constant heat flux, Exp. Therm Fluid Sci. 32 (2008) 1638–1646.
[31] K. Khanafer, K. Vafai, A critical synthesis of thermophysical characteristics of nanofluids, Int. J. Heat Mass Transf. 54 (2011) 4410–4428.
[32] H.R. Seyf, Z. Zhou, H. Ma, Y. Zhang, Three dimensional numerical study of heat-transfer enhancement by nano-encapsulated phase change material slurry in microtube heat sinks with tangential impingement, Int. J. Heat Mass Transf. 56 (2013) 561–573.
[33] A. Zaraki, M. Ghalambaz, A.J. Chamkha, M. Ghalambaz, D. De Rossi, Theoretical analysis of natural convection boundary layer heat and mass transfer of nanofluids: Effects of size, shape and type of nanoparticles, type of base fluid and working temperature, Adv. Powder Technol. 26 (2015) 935–946.
[34] M. Ghalambaz, A. Doostani, E. Izadpanahi, A.J. Chamkha, Phase-change heat transfer in a cavity heated from below: the effect of utilizing single or hybrid nanoparticles as additives, J. Taiwan Inst. Chem. Eng. 72 (2017) 104–115.
[35] J.N. Reddy, An introduction to the finite element method, New York, 1993
[36] K. Kahveci, Buoyancy driven heat transfer of nanofluids in a tilted enclosure, J. Heat Transfer 132 (2010) 062501.
[37] F. Xu, J.C. Patterson, C. Lei, Heat transfer through coupled thermal boundary layers induced by a suddenly generated temperature difference, Int. J. Heat Mass Transf. 52 (2009) 4966–4975.